Journal of Solid Mechanics Vol. 8, No. 3 (2016) pp. 625-644

Deformation Due to Inclined Loads in Thermoporoelastic Half Space

R. Kumar [1], S.Kumar [2, *], M. G. Gorla [3]

[1]*Department of Mathematics, Kurukshetra University, Kurukshetra, Haryana, India*
[2]*Department of Mathematics, Govt. Degree College Chowari (Chamba), Himachal Pradesh, India*
[3]*Department of Mathematics, Himachal Pradesh University, Shimla-171005, India*

Received 28 June 2016; accepted 25 August 2016

ABSTRACT

The present investigation is concerned with the deformation of thermoporoelastic half space with incompressible fluid as a result of inclined load of arbitrary orientation. The inclined load is assumed to be linear combination of normal load and tangential load. The Laplace and Fourier transform technique are used to solve the problem. The concentrated force, uniformly distributed force and a moving force in time and frequency domain are taken to illustrate the utility of the approach. The transformed components of displacement, stress, pore pressure and temperature change are obtained and inverted by using a numerical inversion techniques. The variations of resulting quantities are depicted graphically. A particular case has also been deduced.

Keywords : Inclined load;Time and frequency domain; Laplace and fourier transform.

1 INTRODUCTION

POROELASTISITY is the mechanics of poroelastic solids with pores filled with fluid. Mathematical theory of poroelastisity deals with the mechanical behaviour of fluid saturated porous medium. Pore fluid generally includes gas, water and oil. Due to different motions of solid and fluid phases and complicated geometry of pore structures, it is very difficult to study the mechanical behaviour of a fluid saturated porous medium. The discovery of fundamental mechanical effects in saturated porous solids and the formulation of the first porous media theories are mainly due to Fillunger [1] ,Terzaghi [2,3 ,4] and their successors.

Based on the work of Von Terzaghi [2,3], Biot [5] proposed a general theory of three dimensional consolidation. Taking the compressibility of the soil into consideration, the water contained in the pores was taken to be incompressible. Biot [6,7] developed the theory for the propagation of stress waves in porous elastic solids containing a compressible viscous fluid and demonstrated the existence of two types of compressional waves (a fast and a slow wave) along with one share wave. Biot's model was broadly accepted and some of his results have been taken as standard references and the basis for subsequent analysis in acoustic, geophysics and other such fields.

For the thermoporoelastisity problems, coupled thermal and poro-mechanical processes play an important role in a number of problems of interest in the geomechanics such as stability of boreholes and permeability enhancement in geothermal reservoirs. A thermoporoelastic approach combines the theory of heat conduction with poroelastic constitutive equations and coupling the temperature fields with the stresses and pore pressure.

Rice and Cleary [8] presented some basic stress-diffusion solutions for fluid saturated elastic porous media with compressible constituents. There exists a substantial literature treating the extension of the well known isothermal

*Corresponding author.
E-mail address: satinderkumars@gmail.com (S. Kumar).

theory to account for the effects of thermal expansion of both the pore fluid and the elastic matrix [eg. Schiffman[9], Bowen[10], Noorishad [11]].

McTigue [12] developed a linear theory of fluid saturated porous thermoelastic material and this theory allows compressibility and thermal expansion of both the fluid and solid constituents. He presented a general solution scheme in which a diffusion equation with temperature dependent source term governs a combination of the mean total stress and the fluid pore pressure.

Kurashige[13] extends the Rice and Cleary [8] theory to incorporate the heat transportation by a pore fluid flow in addition to the effect of difference in expansibility between the pore fluid and the skeletal solid and presented a thermoelastic theory of fluid-filled porous materials. This theory shows that the displacement field is completely coupled with the pore pressure and temperature field in general, however, for irrotational displacement; the first field is decoupled from the last two, which are still coupled to each other. This pore pressure-temperature coupling involves nonlinearity.

Abousleiman and Ekbote [14] obtained the solutions for the inclined borehole in a porothermoelastic transversely isotropic medium. Bai [15] studied the fluctuation responses of porous media subjected to cyclic thermal loading. Bai and Li [16] obtained the solution for cylindrical cavity in a saturated thermoporoelastic medium.

Jabbari and Dehbani [17] considered the classical coupled thermoporoelastic model of hollow and solid cylinders under radial symmetric loading conditions and presented a unique solution. Ganbin et al. [18] obtained the solution in saturated porous thermoviscoelastic medium, with cylindrical cavity that is subjected to time dependent thermal load by using Laplace transform technique. Gatmiri et al. [19] presented the two-dimensional fundamental solutions for non-isothermal unsaturated deformable porous medium subjected to quasi- static loading in time and frequency domain. Li et al. [20] presented the study state solutions for transversely isotropic thermoporoelastic media in three dimensions.

Jabbari and Dehbani [21] considered the quasi- static porothermoelasticity model of hollow and solid sphere and obtained the displacement, temperature distribution and pressure distribution due mechanical, thermal and pressure source. Liu et al. [22] studied the relaxation effect of a saturated porous media using the two dimensional generalized thermoelastic theory. Belotserkovets and Prevost [23] obtained an analytical solution of thermoporoelastic response of fluid-saturated porous sphere.

Bai [24] derived an analytical method for the thermal consolidation of layered saturated porous material subjected to exponential decaying thermal loading. Mixed variation principal for dynamic response of thermoelastic and poroelastic continua was discussed by Apostolakis and Dargus [25]. Hou, et al. [26] discussed the three dimensional Green's function for transversely isotropic thermoporoelastic biomaterial. Jabbari et al. [27] presented the thermal buckling analysis of functionally graded thin circular plate made of saturated porous material and obtained the closed form solutions for circular plates subjected to temperature load.

Liu and Chain [28] discussed a micromechanical analysis of the fracture properties of saturated porous media. He et al. [29] studied the dynamic simulation of landslide based on thermoporoelastic approach. Nguyen et al. [30] discussed the analytical study of freezing behaviour of a cavity in thermoporoelastic medium. Wu et al. [31] presented a refined theory of axisymmetric thermoporoelastic circular cylinder.

Kumar and Ailawalia [32, 33] studied the response of moving inclined load in orthotropic elastic half-space and micropolar elastic half-space with voids respectively . Kumar and Rani [34] studied the general plane strain problem of thermoelastic half-space with voids as a result of inclined load due to different sources. Sharma [35] investigated the deformation in a homogeneous isotropic thermodiffusive elastic half-space as a result of inclined load by assuming the inclined load as a linear combination of normal load and tangential load. Stress-strain state of a inclined elliptical defect in a plate under biaxial loading was discussed by Ostsemin and Utkin [36]. Stress-strain state of an elastic half plane under a system of inclined piecewise - linear loads was studied by Bogomolov and Ushakov [37].

In the present paper, the investigation is concerned with the deformation of thermoporoelastic half space with incompressible fluid as a result of inclined load of arbitrary orientation. The inclined load is assumed to be linear combination of normal load and tangential load. The components of displacement, stress, pore pressure and temperature change are obtained in time and frequency domain. Numerical inversion technique is applied to obtain the resulting quantities in a physical domain. The resulting quantities are shown graphically to depict the effect of porosity

The result of the problem may be applied in the field of engineering and geophysical problems involving temperature change. The physical applications are encounter in the context of problems like ground explosion, oil industries etc. This problem is also useful in the field of geomechanics, where the interest is about the various phenomenon occurring in the earthquakes and measuring the components of displacement, stress, pore pressure and

temperature change due to the presence of certain sources. Also the present investigation is useful to study the deformation field around mining tremors and drilling into the crust of the earth. It also contributes to the theoretical consideration of the seismic sources because it can account for the deformation fields in the entire volume surrounding the sources region.

2 BASIC EQUATIONS

Following Jabbari and Dehbani [38], the basic equations are

$$(\lambda+\mu)\nabla\nabla.\vec{u}+\mu\nabla^2\vec{u}-\alpha\nabla p-\beta\nabla T=\rho\frac{\partial^2\vec{u}}{\partial t^2} \tag{1}$$

$$\frac{k}{\gamma_w}\nabla^2 p-\alpha_p\dot{p}-Y\dot{T}-\alpha div\,\dot{\vec{u}}=0 \tag{2}$$

$$K\nabla^2 T-ZT_0\dot{T}+YT_0\dot{p}-\beta T_0 div\,\dot{\vec{u}}=0 \tag{3}$$

$$\sigma_{ij}=\lambda u_{k,k}\delta_{ij}+\mu(u_{i,j}+u_{j,i})-\alpha p\delta_{ij}-\beta T\delta_{ij} \tag{4}$$

where $\vec{u}$ is the displacement component, p is the pore pressure, ρ is the bulk mass density, $\alpha=1-\frac{C_s}{C}$ is the Biot's coefficient, $C_s=\frac{3(1-2\nu_s)}{E_s}$ is the coefficient of volumetric compression of solid grain, with E_s and ν_s being the elastic modulus and Poisson's ratio of solid grain, $C=\frac{3(1-2\nu)}{E}$ is the coefficient of volumetric compression of solid skeleton, with E and ν being the elastic modulus and Poisson's ratio of solid skeleton, T_0 is initial reference temperature, $\beta=\frac{3\alpha_s}{C}$ is the thermal expansion factor, α_s is the coefficient of linear thermal expansion of solid grain, $Y=3(n\alpha_w+(\alpha-n)\alpha_s)$ and $\alpha_p=n(C_w-C_s)+\alpha C_s$ are coupling parameters, α_w and C_w are the coefficients of linear thermal expansion and volumetric compression of pure water, n is the porosity, k is the hydraulic conductivity, γ_w is the unit of pore water and $Z=\frac{(1-n)\rho_s C_s+n\rho_w C_w}{T_0}$ is coupling parameter, ρ_w and ρ_s are densities of pore water and solid grain and C_w and C_s are heat capacities of pore water and solid grain and K is the coefficient of heat conductivity.

3 FORMULATION OF THE PROBLEM

We consider homogeneous, isotropic, poroelastic thermal conducting half space $x_3\geq 0$ of a rectangular Cartesian coordinate system (x_1,x_2,x_3) having origin at the surface $x_3=0$ and x_3 – axis pointing vertically downward in the medium has been taken. We take an inclined load F_0, per unit length, is acting along the interface on x_1 axis and its inclination with x_3 axis is θ. The complete geometry of the problem is shown in the Fig. 1(a), 1(b),1(c),1(d) and 1(e).

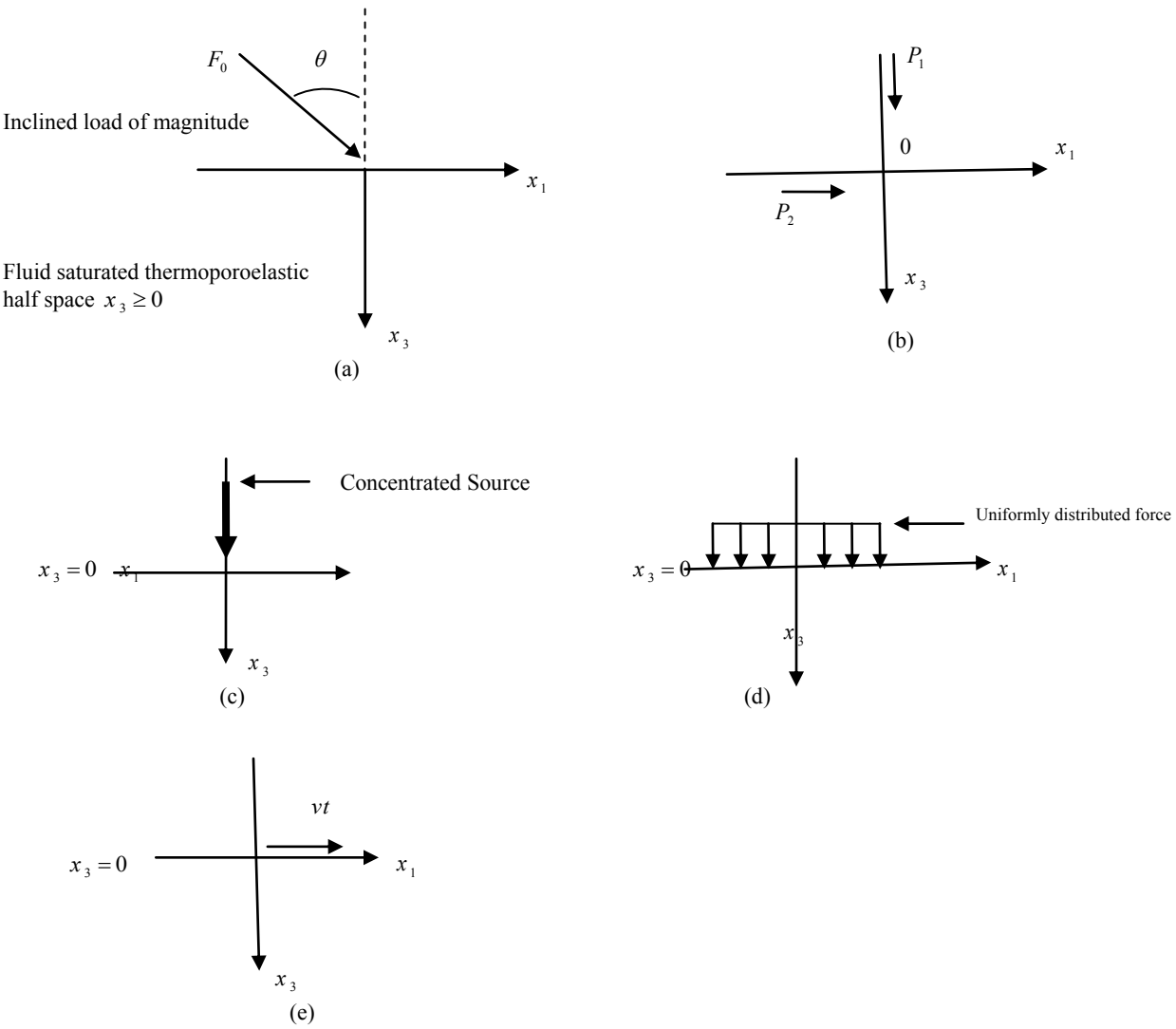

Fig.1
a) Inclined load on the fluid saturated thermoporoelastic half space. b) Components of the inclined load. c) Concentrated force on the fluid saturated thermoporoelastic half space. d) Uniformly distributed force on the fluid saturated thermoporoelastic half space.e) Moving force on the fluid saturated thermoporoelastic half space.

For two dimensional problem, we assume the displacement vector $\vec{u}$ as:

$$\vec{u} = (u_1, 0, u_3) \tag{5}$$

For further consideration it is convenient to introduce the dimensionless quantities defined as:

$$\begin{aligned} &x_1' = \frac{\omega^*}{c_1} x_1, x_3' = \frac{\omega^*}{c_1} x_3, u_1' = \frac{\omega^* \rho c_1}{\beta T_0} u_1, u_3' = \frac{\omega^* \rho c_1}{\beta T_0} u_3, p' = \frac{p}{\beta T_0}, c_1^2 = \frac{\lambda + 2\mu}{\rho}, \\ &t' = \omega^* t, T' = \frac{T}{T_0}, \omega^* = \frac{Z T_O c_1^2}{K}, \sigma_{33}' = \frac{\sigma_{33}}{\beta T_0}, \sigma_{31}' = \frac{\sigma_{31}}{\beta T_0} \end{aligned} \tag{6}$$

where ω^* is a constant having the dimensions of frequency.

The displacement components u_1 and u_3 are related to the potential functions $\Phi(x_1, x_3, t), \Psi(x_1, x_3, t)$ as:

$$u_1 = \frac{\partial \Phi}{\partial x_1} - \frac{\partial \Psi}{\partial x_3}, u_3 = \frac{\partial \Phi}{\partial x_3} + \frac{\partial \Psi}{\partial x_1} \tag{7}$$

Making use of (5) on (1)-(3) and using the dimensionless quantities given by (6), on the resulting quantities and with the aid of (7), after suppressing the prime, yield

$$(1+a_1)\nabla^2\Phi - a_2 p - a_3 T - a_3 \frac{\partial^2 \Phi}{\partial t^2} = 0 \tag{8}$$

$$a_1 \nabla^2 \Psi - a_3 \frac{\partial^2 \Psi}{\partial t^2} = 0 \tag{9}$$

$$b_1 \nabla^2 p - b_2 \frac{\partial p}{\partial t} - b_3 \frac{\partial T}{\partial t} - \frac{\partial}{\partial t}[\nabla^2 \Phi] = 0 \tag{10}$$

$$b_4 \nabla^2 T - b_5 \frac{\partial T}{\partial t} + b_6 \frac{\partial p}{\partial t} - \frac{\partial}{\partial t}[\nabla^2 \Phi] = 0 \tag{11}$$

where

$$a_1 = \frac{\mu}{\lambda+\mu}, a_2 = \frac{\alpha \rho c_1^2}{\lambda+\mu}, a_3 = \frac{\rho c_1^2}{\lambda+\mu}, b_1 = \frac{k\,\omega^* \rho}{\gamma_w \alpha}, b_2 = \frac{\alpha_p \rho c_1^2}{\alpha}$$
$$b_3 = \frac{Y\,\rho c_1^2}{\alpha\beta}, b_4 = \frac{K\,\omega^* \rho}{\beta^2 T_0}, b_5 = \frac{Z\,\rho c_{10}^2}{\beta^2}, b_6 = \frac{Y\,\rho c_1^2}{\beta^2}, e = \frac{\partial u_1}{\partial x_1} + \frac{\partial u_3}{\partial x_3}$$

We define the Laplace and Fourier transforms as follows:

$$\bar{f}(x_1, x_3, s) = \int_0^\infty f(x_1, x_3, t) e^{-st} dt \tag{12}$$

$$\tilde{\bar{f}}(\xi, x_3, s) = \int_{-\infty}^{\infty} \bar{f}(x_1, x_3, s) e^{i\xi x_1} dx \tag{13}$$

Applying Laplace and Fourier transforms defined by (12) and (13) on Eqs. (8)-(11) and eliminating $\tilde{\bar{p}}$ and $\tilde{\bar{T}}$ from resulting equations, we obtain

$$[A_1 \frac{d^6}{dx_3^6} + A_2 \frac{d^4}{dx_3^4} + A_3 \frac{d^2}{dx_3^2} + A_4]\tilde{\bar{\Phi}} = 0 \tag{14}$$

$$[\frac{d^2}{dx_3^2} - A_5]\tilde{\bar{\Psi}} = 0 \tag{15}$$

where

$$A_1 = b_1 b_4 (1+a_1),$$
$$A_2 = -3\xi^2 b_1 b_4 (1+a_1) - s(1+a_1)(b_1 b_5 + b_2 b_4) - a_3 b_1 b_4 s^2 - a_2 b_4 s - a_3 b_1 s,$$
$$A_3 = -3\xi^4 b_1 b_4 (1+a_1) - 2\xi^2 s (1+a_1)(b_1 b_5 + b_2 b_4) + s^2 (1+a_1)(b_1 b_5 + b_2 b_4) + 2\xi^2 s^2 a_3 b_1,$$

$$A_4 = -\xi^6 b_1 b_4 (1+a_1) - s\xi^4 (1+a_1)(b_1 b_5 + b_2 b_4) + s^2 \xi^2 (1+a_1)(b_1 b_5 + b_2 b_4) - a_3 b_1 b_4,$$

$$\mathrm{A}_5 = \xi^2 + \frac{a_3}{a_1} s^2.$$

Solving (14) and (15) and assuming that $\tilde{\bar{\Phi}}, \tilde{\bar{\Psi}}, \tilde{\bar{p}}$ and $\tilde{\bar{T}} \to 0$ as $x_3 \to \infty$ we obtain the value of $\tilde{\bar{\Phi}}, \tilde{\bar{\Psi}}, \tilde{\bar{p}}$ and $\tilde{\bar{T}}$ as:

$$(\tilde{\bar{\Phi}}, \tilde{\bar{p}}, \tilde{\bar{T}}) = \sum_{i=1}^{3} (1, r_i, s_i) \mathrm{B}_1 \mathrm{e}^{-\mathrm{m}_i x_3} \tag{16}$$

$$\tilde{\bar{\Psi}} = \mathrm{B}_4 \mathrm{e}^{-\mathrm{m}_4 x_3} \tag{17}$$

where $\mathrm{m}_1, \mathrm{m}_2, \mathrm{m}_3$ are the roots of the Eq. (16) and $\mathrm{m}_4 = \sqrt{\mathrm{A}_5}$. The coupling constants are given by

$$\mathrm{r}_i = \frac{b_4 s (m_i^2 - \xi^2)^2 + (b_3 s^2 - b_5 s^2)(m_i^2 - \xi^2)}{b_1 b_4 (m_i^2 - \xi^2)^2 - s(b_1 b_5 + b_2 b_4)(m_i^2 - \xi^2) + s^2 (b_2 b_5 + b_3 b_6)} \tag{18}$$

$$\mathrm{s}_i = \frac{b_1 s (m_i^2 - \xi^2)^2 - (b_6 s^2 + b_2 s^2)(m_i^2 - \xi^2)}{b_1 b_4 (m_i^2 - \xi^2)^2 - s(b_1 b_5 + b_2 b_4)(m_i^2 - \xi^2) + s^2 (b_2 b_5 + b_3 b_6)} \qquad (i = 1,2,3) \tag{19}$$

The displacement components $\tilde{\bar{u}}_1$ and $\tilde{\bar{u}}_3$ are obtained with the aid of (12)-(13) and (16)-(17) as:

$$\tilde{\bar{u}}_1 = -B_1 i\xi e^{-m_1 x_3} - B_2 i\xi e^{-m_2 x_3} - B_3 i\xi e^{-m_3 x_3} + B_4 m_4 e^{-m_4 x_3} \tag{20}$$

$$\tilde{\bar{u}}_3 = -B_1 m_1 e^{-m_1 x_3} - B_2 m_2 e^{-m_2 x_3} - B_3 m_3 e^{-m_3 x_3} - B_4 i\xi e^{-m_4 x_3} \tag{21}$$

4 BOUNDARY CONDITIONS

The boundary conditions at $x_3 = 0$ are

$$\sigma_{33} = -P_1 F(x_1, t), \sigma_{31} = -P_2 F(x_1, t), p = 0, \frac{\partial T}{\partial x_3} = 0 \tag{22}$$

where P_1, P_2 are the magnitudes of the forces and $F(x_1, t)$ is a known function of x_1 and t.

Applying Laplace and Fourier transforms defined by (12) and (13) on (22) and with the aid of (4),(6) along with $P_1' = \frac{P_1}{\beta T_0}, P_2' = \frac{P_2}{\beta T_0}$ (after suppressing the prime), we obtain

$$\tilde{\bar{\sigma}}_{33} = -P_1 \tilde{\bar{F}}(\xi, s), \tilde{\bar{\sigma}}_{31} = -P_2 \tilde{\bar{F}}(\xi, s), \tilde{\bar{p}} = 0, \frac{\partial \tilde{\bar{T}}}{\partial x_3} = 0 \ , \quad at \quad x_3 = 0 \tag{23}$$

where

$$\tilde{\bar{\sigma}}_{33} = -R_1 i\xi \tilde{\bar{u}}_1 + R_2 \frac{d\tilde{\bar{u}}_3}{dx_3} - \alpha \tilde{\bar{p}} - \beta \tilde{\bar{T}} \tag{24}$$

$$\tilde{\tilde{\sigma}}_{31} = R_3[\frac{d\tilde{\tilde{u}}_1}{dx_3} - i\,\xi\tilde{\tilde{u}}_3] \tag{25}$$

and $R_1 = \frac{\lambda}{\rho c_1^2}, R_2 = \frac{\lambda + 2\mu}{\rho c_1^2}, R_3 = \frac{\mu}{\rho c_1^2}$.

Substituting the values of $\tilde{\tilde{u}}_1, \tilde{\tilde{u}}_3, \tilde{\tilde{p}}$ and $\tilde{\tilde{T}}$ from (20),(21) and (16) in the boundary condition (23) and with help of (24) and (25), after some simplifications, we obtain

$$\tilde{\tilde{\sigma}}_{33} = \frac{\tilde{\tilde{F}}}{\Delta}[d_1\Delta_1 e^{-m_1 x_3} + d_2\Delta_2 e^{-m_2 x_3} + d_3\Delta_3 e^{-m_3 x_3} + d_4\Delta_4 e^{-m_4 x_3}] \tag{26}$$

$$\tilde{\tilde{\sigma}}_{31} = \frac{\tilde{\tilde{F}}}{\Delta}[d_5\Delta_1 e^{-m_1 x_3} + d_6\Delta_2 e^{-m_2 x_3} + d_7\Delta_3 e^{-m_3 x_3} + d_8\Delta_4 e^{-m_4 x_3}] \tag{27}$$

$$(\tilde{\tilde{p}}, \tilde{\tilde{T}}) = \frac{\tilde{\tilde{F}}}{\Delta}\sum_{i=1}^{3}(r_i, s_i)\Delta_i e^{-m_i x_3} \tag{28}$$

where

$$\Delta = d_1 d_8(-m_3 r_2 s_3 + m_2 r_3 s_2) - d_2 d_8(-m_3 r_1 s_3 + m_1 r_3 s_1) + d_3 d_8(-m_2 r_1 s_2 + m_1 r_2 s_1)$$
$$-d_4 d_5(-m_3 r_2 s_3 + m_2 r_3 s_2) - d_4 d_6(-m_1 r_3 s_1 + m_3 r_1 s_3) - d_4 d_7(-m_2 r_1 s_2 + m_1 r_2 s_1)$$

$d_i = -R_1\xi^2 + R_2 m_i^2 - \alpha r_i - s_i$ where $(i = 1,2,3), d_4 = i\,\xi m_4(-R_1 + R_2)$
$d_j = 2i\,\xi m_j R_3$ where $(j = 5,6,7), d_8 = -R_3(m_4^2 + \xi^2)$

and $\Delta_1, \Delta_2, \Delta_3, \Delta_4$ are obtained by replacing $[-P_1, -P_2, 0, 0]^T$ in Δ.

5 APPLICATIONS

5.1 Inclined loads

For an inclined load F_0, per unit length, we have

$$P_1 = F_0\cos\theta, P_2 = F_0\sin\theta \tag{29}$$

Using (29) in Eqs. (26)-(28), we obtain the corresponding expression for stresses, pore pressure and temperature in case of inclined load on the surface of half space.

5.1.1 Time domain

The expressions of stress component, pore pressure and temperature change are in transformed variable in which $F(x_1, t)$ is an unknown function. A different class of sources is represented by setting,

$$F(x_1, t) = F_1(x_1)\eta(t) \tag{30}$$

where $\eta(t) = H(t)$, where $H()$ Heaviside unit step function , $F_1(x_1)$ is a known function and takes two types of value representing the two different sources as,

Concentrated force:

$$F_1(x_1) = \delta(x_1) \tag{31}$$

where $\delta()$ is the Dirac-delta function.

Uniformly distributed force:

$$F_1(x_1) = H(x_1 + a) - H(x_1 - a) \tag{32}$$

Applying the Laplace and Fourier transform defined by (12) and (13) on (30), with the aid of (31) and (32), yield

$$\tilde{\bar{F}}(\xi, s) = 1/s \tag{33}$$

For concentrated force, and

$$\tilde{\bar{F}}(\xi, s) = [(2\sin \xi a)/s\xi] \tag{34}$$

For distributed force.

Moving force:

$$F(x_1, t) = \delta(x_1 - vt)\eta(t) \tag{35}$$

where v is the uniform speed of the impulsive force at $x_3 = 0$.

Applying the Laplace and Fourier transform defined by (12) and (13) on (35), we obtain

$$\tilde{\bar{F}}(\xi, s) = 1/(s - i v\xi) \tag{36}$$

The expression for stress component, pore pressure and temperature change can be obtained for concentrated force, distributed forces and moving force by replacing $\tilde{\bar{F}}(\xi, s)$ from (33),(34) and (36) in (26)-(28).

5.1.2 Frequency domain

In this case, we assume the time harmonic behaviour as,

$$(u_1, u_3, p, T)(x_1, x_3, t) = (u_1, u_3, p, T)(x_1, x_3)e^{i\omega t}$$

In frequency domain, we take

$$\eta(t) = e^{i\omega t} \tag{37}$$

The expressions for stresses, pore pressure and thermal source in frequency domain can be obtained by replacing s by $i\omega$ in the expressions of time domain along with $\bar{\eta}(s)$ to be replaced by $e^{i\omega t}$ for concentrated and distributed force.

The solution due to impulsive harmonic force, moving with uniform dimensionless speed v at $x_3 = 0$ is obtained by replacing $F(x_1, t)$ with $\delta(x_1 - vt)$, whose Fourier transform is $e^{i\xi vt}$.

5.2 Special case

In the absence of porosity effect, the boundary conditions reduce to

$$\tilde{\tilde{\sigma}}_{33} = -P_1\tilde{\tilde{F}}(\xi,s), \tilde{\tilde{\sigma}}_{31} = -P_2\tilde{\tilde{F}}(\xi,s), \frac{\partial\tilde{\tilde{T}}}{\partial x_3} = 0 \tag{38}$$

and we obtain the corresponding expressions for stress components and temperature change in thermoelastic elastic half space as:

$$\tilde{\tilde{\sigma}}_{33} = \frac{\tilde{\tilde{F}}}{\Delta_{10}}[d_9\Delta_5 e^{-m_5x_3} + d_{10}\Delta_6 e^{-m_6x_3} + d_4\Delta_7 e^{-m_7x_3}] \tag{39}$$

$$\tilde{\tilde{\sigma}}_{31} = \frac{\tilde{\tilde{F}}}{\Delta_{10}}[d_{11}\Delta_5 e^{-m_5x_3} + d_{12}\Delta_6 e^{-m_6x_3} + d_8\Delta_7 e^{-m_7x_3}] \tag{40}$$

$$\tilde{\tilde{T}} = \frac{\tilde{\tilde{F}}}{\Delta_{10}}[r_5\Delta_5 e^{-m_5x_3} + r_6\Delta_6 e^{-m_6x_3}] \tag{41}$$

where

$$\Delta_{10} = d_9d_8m_6r_6 - d_{10}d_8m_5r_5 - d_4d_{11}m_6r_6 + d_4d_{12}m_5r_5$$
$$d_9 = -R_1\xi^2 + R_2m_5^2 - r_5, d_{10} = -R_1\xi^2 + R_2m_6^2 - r_6, d_{11} = 2i\,\xi m_5R_3, d_{12} = 2i\,\xi m_6R_3,$$
$$\mathrm{r_i} = \frac{s(m_i^2 - \xi^2)}{b_4(m_i^2 - \xi^2) - b_5s}(i = 5,6)$$

and $\Delta_5, \Delta_6, \Delta_7$ are obtained by replacing $[-P_1, -P_2, 0]^T$ in Δ_{10}.

The results obtained in (39)-(41) are similar if we solve the problem in thermoelastic half space due to inclined load of arbitrary orientation.

5.3 Inversion of the transform

The transformed stresses, pore pressure and temperature are functions of the parameters of the Laplace and Fourier transforms s and ξ respectively and hence are of the form $\tilde{\tilde{f}}(\xi, x_3, s)$. To obtain the solution of the problem in the physical domain, we invert the Laplace and Fourier transforms by using the method described by Kumar et al. [39].

6 NUMERICAL RESULTS AND DISCUSSION

With the view of illustrating the theoretical results and for numerical discussion we take a model for which the value of the various physical parameters is taken from Jabbari and dehbani [38]:

$$E = 6\times10^5\,\mathrm{Pa}, \nu = 0.3, T_0 = 293°\mathrm{K}, K_s = 2\times10^{10}\,Pa, K_w = 5\times10^9\,Pa, K = 0.5,$$
$$\alpha_s = 1.5\times10^{-5}\,1/{}^0C, \alpha_w = 2\times10^{-4}\,1/{}^0C, c_s = 0.8\mathrm{J/g}\,{}^0C, c_w = 4.2\mathrm{J/g}\,{}^0C, \rho_s = 2.6\times10^6\,g/m^3,$$
$$\rho_w = 1\times10^6\,g/m^3, n = 0.4, \alpha = 1, P_1 = P_2 = 1, t = 0.5$$

The variation of normal stress σ_{33}, tangential stress σ_{31}, pore pressure p and temperature change T for incompressible fluid saturated thermoporoelastic medium (FSPM) and empty porous thermoelastic medium (EPM) are shown in Figs. 2-25 due to concentrated force (CS), uniformly distributed force (UDS), and moving force. In all these figures, solid line (___), solid line with central symbol (- o - o -) and solid line with central symbol (- x – x -) corresponds to the variations at $\theta = 0^0, 45^0, 90^0$ respectively. Similarly small dashed line (------), small dashed line

with central symbol (- o - o -) and small dashed line with central symbol (- x – x -) correspond to the variations at $\theta = 0^0, 45^0, 90^0$ respectively. The computation is carried out at $x_3 = 1$ for the range $0 \le x_1 \le 10$. All the results are shown for one value of dimensionless width $a = 1$ and one value of dimensionless velocity $V = 1$.

6.1 Time domain

Figs. 2-13 show the variations due to concentrated force, uniformly distributed force and moving force respectively. Fig.2 shows the variation of normal stress component σ_{33} for both FSPM and EPM. The value of σ_{33} for FSPM increases in the range $0 \le x_1 \le 3$ for $\theta = 0^0$, 45^0 and then oscillates with large magnitude, whereas for $\theta = 90^0$ first increases and then decreases x_1 increases. The value of σ_{33} for EPM, first increases in the range $0 \le x_1 \le 2.2$ and then oscillates with small magnitude when $\theta = 0^0, 45^0$ and for $\theta = 90^0$ its value converges near the boundary surface.

Fig.3 shows the variation of tangential stress component σ_{31} for both FSPM and EPM. The value of σ_{31} for FSPM oscillates for all values of θ with large magnitude as x_1 increases, while for EPM, the value of σ_{31} decreases in the range $0 \le x_1 \le 2.2$ and then oscillates with small magnitude for all values of θ as x_1 increase.

Fig.4 and Fig.8 show the variation of pore pressure p for FSPM. The value of p for FSPM first decreases in the range $0 \le x_1 \le 3.2$ when $\theta = 0^0, 45^0$ and increases in the range $3.2 \le x_1 \le 9$ and then decreases as x_1 increases whereas for extreme angle, with small initial increase, the value of p decreases in the range $1.5 \le x_1 \le 4$ and then increases as x_1 increases.

Behaviour of temperature *T* for FSPM and EPM is shown in Fig.5. The value of *T* for FSPM, when $\theta = 0^0, 45^0$, increases in the range $0 \le x_1 \le 3.2$ and then oscillates whereas, for extreme angle, the value of *T* oscillates about the origin as x_1 increases. For EPM, the value of *T* decreases as x_1 increases when $\theta = 0^0, 45^0$ whereas for $\theta = 90^0$, it decreases in the range $0 \le x_1 \le 2.1$ and then converges near the boundary surface as x_1 increases.

Fig.6 depicts the variation of normal stress component σ_{33} for both FSPM and EPM. The value of σ_{33} for FSPM increases in the range $0 \le x_1 \le 3$ for $\theta = 0^0, 45^0$ and then oscillates with large magnitude whereas for $\theta = 90^0$ it increases and then decreases as x_1 increases. In case of EPM, the value of σ_{33} , when $\theta = 0^0, 45^0$ first increases in the range $0 \le x_1 \le 2.2$ and then oscillates about the origin and for $\theta = 90^0$ its value first increases and then converges near the boundary surface.

Fig.7 shows the variation of tangential stress component σ_{31} for both FSPM and EPM. The value of σ_{31} for FSPM increases in the range $0 \le x_1 \le 2$ for initial angle and increases in the range $0 \le x_1 \le 2.5$ for intermediate and extreme angles and then oscillates with large magnitude as x_1 increases. In case of EPM, the value of σ_{31} decreases in the range $0 \le x_1 \le 2$ and then oscillates with small magnitude for all values of θ as x_1 increases.

Fig.9 shows the variation of temperature *T* for both FSPM and EPM. The value of *T* for FSPM increases in the range $0 \le x_1 \le 3.5$ for initial and intermediate angles and then oscillates whereas for extreme angle its value oscillates as x_1 increases. In case of EPM, the value of *T* decreases exponentially for initial and intermediate angles and converges near the boundary surface for extreme angle as x_1 increases.

Fig.10 depicts the variation of tangential stress component σ_{33} for both FSPM and EPM. The value of σ_{33} for FSPM increases in the range $0 \le x_1 \le 3$ for $\theta = 0^0, 45^0$ and then oscillates with large magnitude whereas for $\theta = 90^0$ first increases and then decreases as x_1 increases. The value of σ_{33} for EPM, when $\theta = 0^0, 45^0$ first increases in the range $0 \le x_1 \le 2.2$ and then oscillates about the origin and for $\theta = 90^0$ its value first increases and then converges near the boundary surface as x_1 increases.

The variation of tangential stress component σ_{31} for both FSPM and EPM is shown in Fig.11. The value of σ_{31} for FSPM increases in the range $0 \le x_1 \le 2$ for initial angle and increases in the range $0 \le x_1 \le 2.5$ for intermediate and extreme angles and then oscillates with large magnitude as x_1 increases. In case of EPM, the value of σ_{31}

decreases in the range $0 \le x_1 \le 2$ and then oscillates with small magnitude for intermediate and extreme angles whereas for initial angle its value converges near the boundary surface as x_1 increases.

Fig.12 shows the variation of pore pressure p for FSPM. The value of p when $\theta = 0^0, 45^0$ for FSPM first decreases in the range $0 \le x_1 \le 4$ and increases in the range $4 \le x_1 \le 9$ and then decreases as x_1 increases whereas for extreme angle, the value of p decreases in the range $0 \le x_1 \le 4$ and then increases as x_1 increases.

Behaviour of temperature T for FSPM and EPM is shown in Fig. 13. The value of T for FSPM increases in the range $0 \le x_1 \le 3.5$ for $\theta = 0^0, 45^0$ and then oscillates whereas for extreme angle its value oscillates about the origin as x_1 increases. In case of EPM, the value of T decreases gradually for $\theta = 0^0, 45^0$ and converges near the boundary surface for $\theta = 90^0$ as x_1 increases.

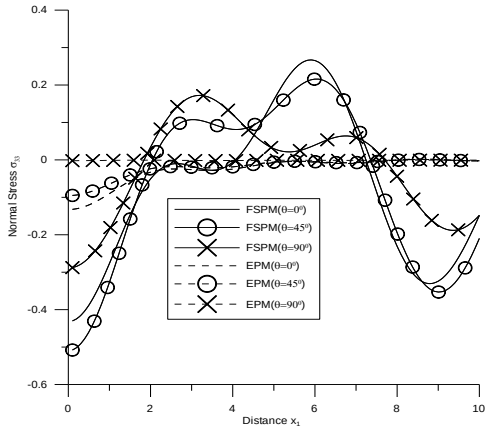

Fig.2
Variation of normal stress σ_{33} w.r.t distance x_1 due to concentrated force.

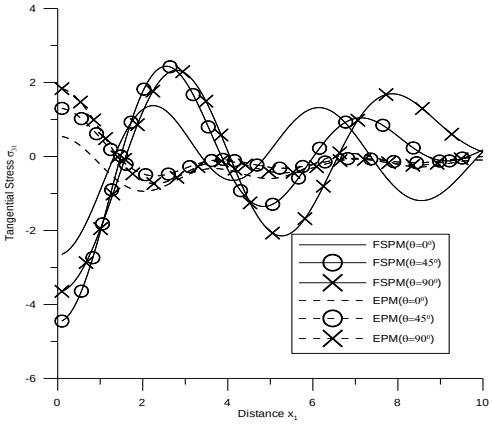

Fig.3
Variation of tangential stress σ_{31} w.r.t distance x_1 due to concentrated force.

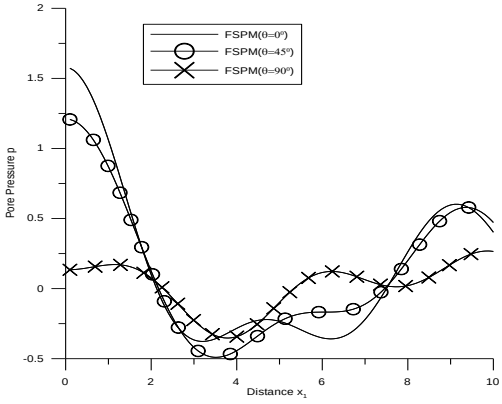

Fig.4
Variation of pore pressure p w.r.t distance x_1 due to concentrated force.

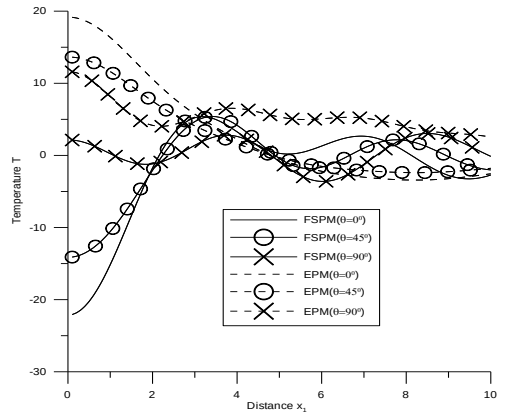

Fig.5
Variation of temperature T w.r.t distance x_1 due to concentrated force.

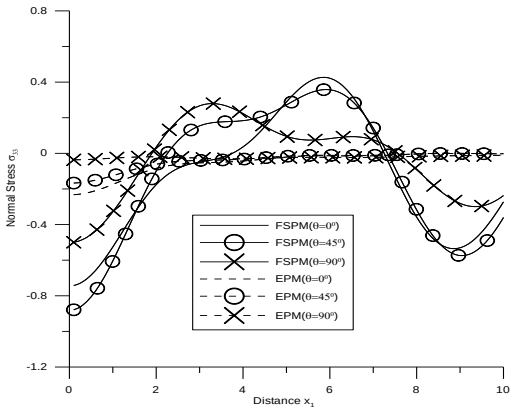

Fig.6
Variation of normal stress σ_{33} w w.r.t distance x_1 due to distributed force.

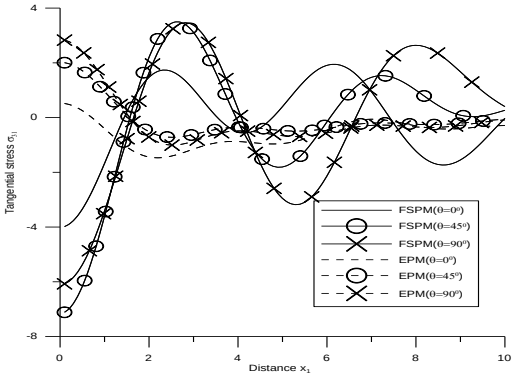

Fig.7
Variation of tangential stress σ_{31} w.r.t distance x_1 due to distributed force.

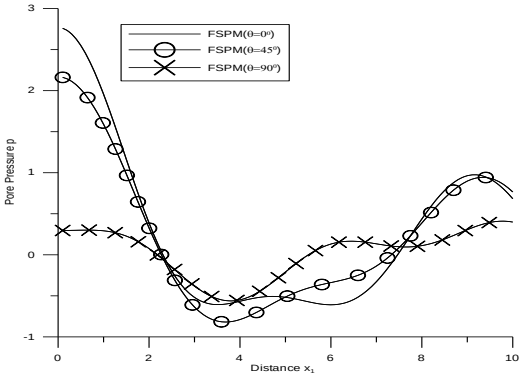

Fig.8
Variation of pore pressure p w.r.t distance x_1 due to distributed force.

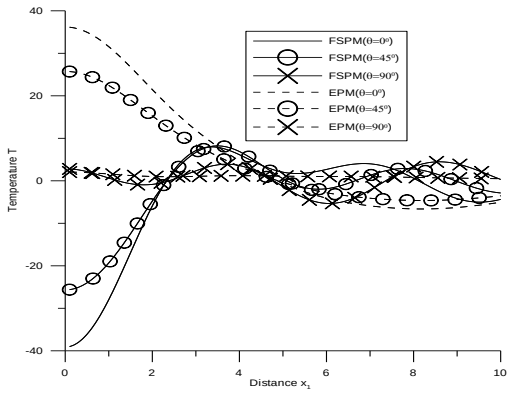

Fig.9
Variation of temperature T w.r.t distance x_1 due to distributed force.

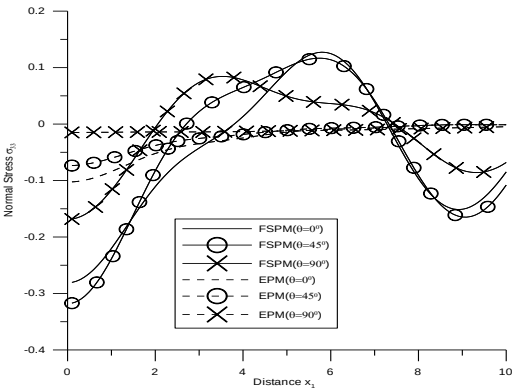

Fig.10
Variation of normal stress σ_{33} w w.r.t distance x_1 due to moving force.

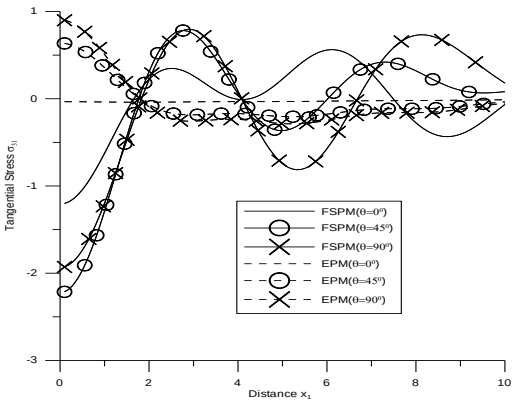

Fig.11
Variation of tangential stress σ_{31} w.r.t distance x_1 due to moving force.

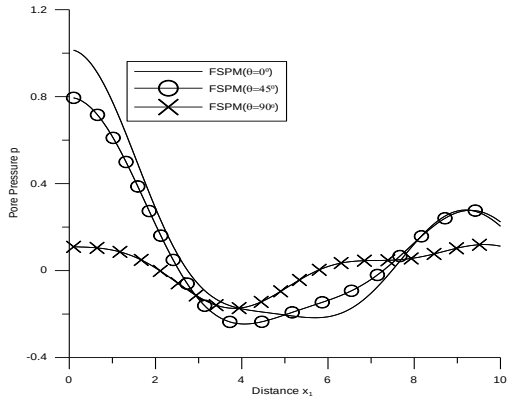

Fig.12
Variation of pore pressure p w.r.t distance x_1 due to moving force.

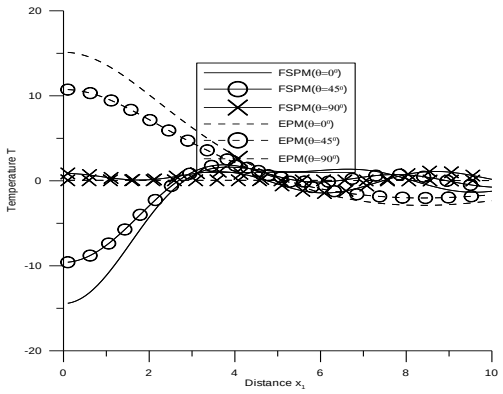

Fig.13
Variation of temperature *T* w.r.t distance x_1 due to moving force.

6.2 Frequency domain

Figs.14-25 show the variations due to concentrated force, uniformly distributed force and moving force respectively. Behaviour of normal stress component σ_{33} for FSPM and EPM is shown in Fig. 14. The value of σ_{33} for FSPM, when $\theta = 0^0, 90^0$ oscillates oppositely in the range $0 \le x_1 \le 5.5$ and then shows the same behaviour whereas for intermediate angle its value oscillates about the origin as x_1 increases. In case of EPM, the value of σ_{33} increases in the range $0 \le x_1 \le 2.2$ and then oscillates with large magnitude whereas for initial angle its value oscillates about the origin as x_1 increases.

Fig.15 depicts the variation of tangential stress component σ_{31} for both FSPM and EPM. The value of σ_{31} for intermediate and extreme angles, for FSPM, oscillates oppositely whereas for initial angle its value oscillates with large magnitude as x_1 increases. In case of EPM, with small initial decrease, the values of σ_{31} converges near the boundary surface for $\theta = 0^0$ whereas for $\theta = 45^0, 90^0$, the values of σ_{31} decreases in the range $0 \le x_1 \le 4.3$ and then oscillates as x_1 increases.

Fig.16 and Fig.20 show the variation of pore pressure *p* for FSPM. The value of *p* for FSPM, when $\theta = 0^0, 90^0$, oscillates oppositely whereas for $\theta = 45^0$ with small initial increase its value decreases in the range $1.5 \le x_1 \le 5.5$, increases in the range $5.5 \le x_1 \le 8.5$ and then decreases as x_1 increases.

Behaviour of temperature *T* for FSPM and EPM is shown in Fig.17. The value of *T* for FSPM, when $\theta = 0^0, 90^0$, oscillates oppositely whereas for $\theta = 45^0$ its value oscillates about the origin as x_1 increases. In case of EPM, for all value of θ, the value of *T* increases in the range $0 \le x_1 \le 4.1$, decreases in the range $4.1 \le x_1 \le 7.1$ and then increases as x_1 increases.

Fig.18 depicts the variation of normal stress component σ_{33} for both FSPM and EPM. The value of σ_{33}, for FSPM, when $\theta = 0^0$ decreases in the range $0 \le x_1 \le 1.2$ and then oscillates whereas for $\theta = 45^0, 90^0$ its value, for both FSPM and EPM, first increases and then oscillates as x_1 increases and when $\theta = 0^0$ in case of EPM, its value first increases and then oscillates as x_1 increases.

Fig.19 shows the variation of tangential stress component σ_{31} for both FSPM and EPM. The value of σ_{31} for intermediate and extreme angles, for FSPM, oscillates oppositely whereas for initial angle its value oscillates with large magnitude as x_1 increases. In case of EPM, with small initial decrease, the values of σ_{31} converges near the boundary surface for $\theta = 0^0$ whereas for $\theta = 45^0, 90^0$, the values of σ_{31} decreases in the range $0 \le x_1 \le 4.3$ and then oscillates as x_1 increases.

Behaviour of temperature *T* for FSPM and EPM is shown in Fig. 21. The value of *T* for FSPM, when $\theta = 0^0, 90^0$, oscillates oppositely whereas for $\theta = 45^0$ its value oscillates about the origin as x_1 increases. In case of EPM, for

all value of θ, the value of T increases in the range $0 \le x_1 \le 4.1$, decreases in the range $4.1 \le x_1 \le 7.1$ and then increases as x_1 increases.

Behaviour of normal stress component σ_{33} for FSPM and EPM is shown in Fig. 22. The value of σ_{33}, for FSPM, when $\theta = 0^0$ decreases in the range $0 \le x_1 \le 1.2$ and then oscillates, whereas for $\theta = 45^0, 90^0$, its value, for both FSPM and EPM, first increases and then oscillates as x_1 increases and when $\theta = 0^0$ in case of EPM, its values first increases and then oscillates as x_1 increases.

Fig.23 depicts the variation of tangential stress component σ_{31} for both FSPM and EPM. The value of σ_{31} for all values of θ oscillate with small magnitude as x_1 increases. In case of EPM, when $\theta = 45^0, 90^0$, the values of σ_{31} decreases in the range $0 \le x_1 \le 4.2$ and then oscillates whereas for $\theta = 0^0$ with small initial decrease its value oscillates as x_1 increases.

Fig.24 shows the variation of pore pressure p for FSPM. The values of p for FSPM oscillates with large magnitude for $\theta = 0^0, 90^0$ and when $\theta = 45^0$, with small initial increase, its value decreases in the range $1.6 \le x_1 \le 5.5$, increases in the range $5.5 \le x_1 \le 8.5$ and then decreases as x_1 increases.

Behaviour of temperature T for FSPM and EPM is shown in Fig. 25. The value of T for FSPM, when $\theta = 0^0, 90^0$, shows the opposite behaviour whereas, for $\theta = 45^0$, with small initial increase, its value decreases in the range $1 \le x_1 \le 5.2$ and then oscillates as x_1 increases. In case of EPM, for all values of θ, the value of T increases in the range $0 \le x_1 \le 4.2$ and then oscillates as x_1 increases.

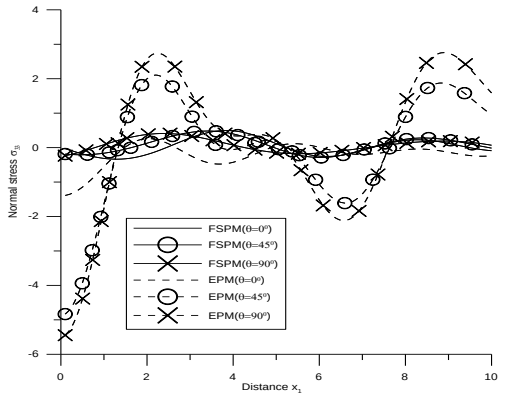

Fig.14
Variation of normal stress σ_{33} w.r.t distance x_1 due to concentrated force (frequency domain).

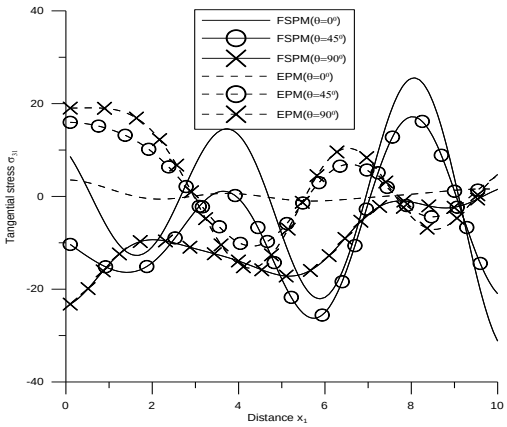

Fig.15
Variation of tangential stress σ_{31} w.r.t distance x_1 due to concentrated force (frequency domain).

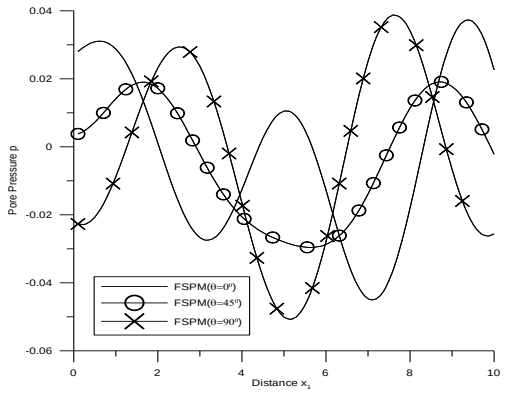

Fig.16
Variation of pore pressure p w.r.t distance x_1 due to concentrated force (frequency domain).

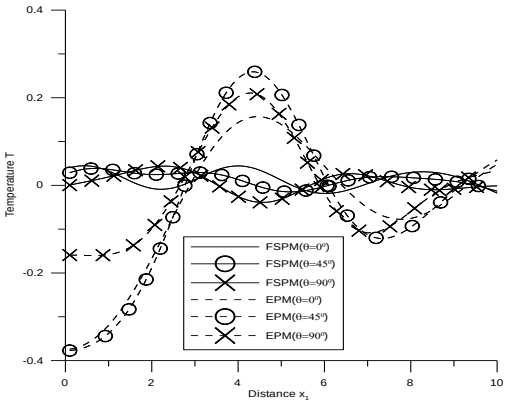

Fig.17
Variation of temperature T w.r.t distance x_1 due to concentrated force(frequency domain).

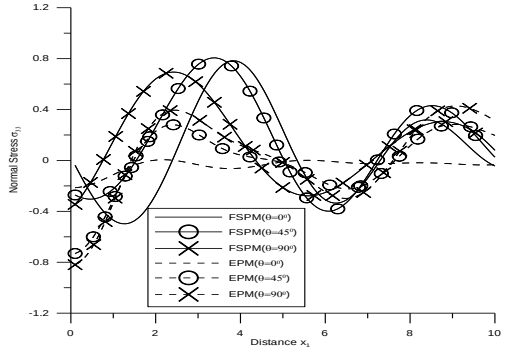

Fig.18
Variation of normal stress σ_{33} w.r.t distance x_1 due to distributed force(frequency domain).

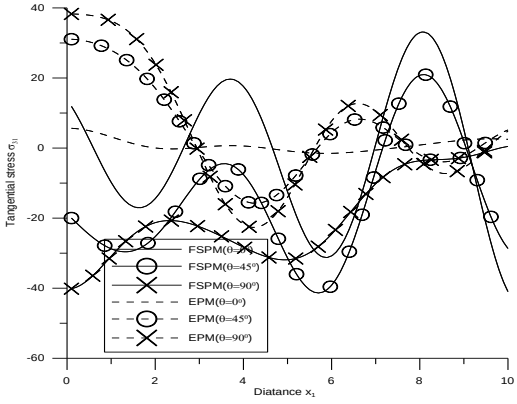

Fig.19
Variation of tangential stress σ_{31} w.r.t distance x_1 due to distributed force(frequency domain).

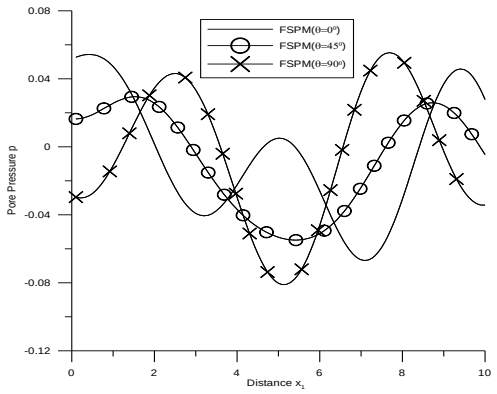

Fig.20
Variation of pore pressure p w.r.t distance x_1 due to distributed force (frequency domain).

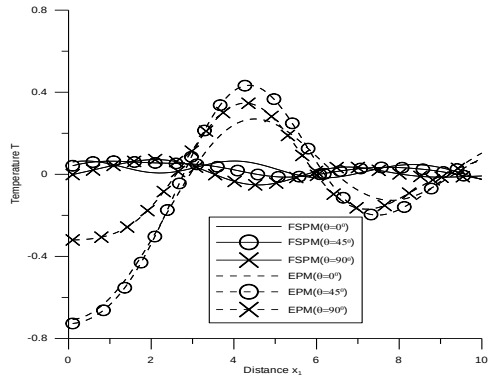

Fig.21
Variation of temperature T w.r.t distance x_1 due to distributed force(frequency domain).

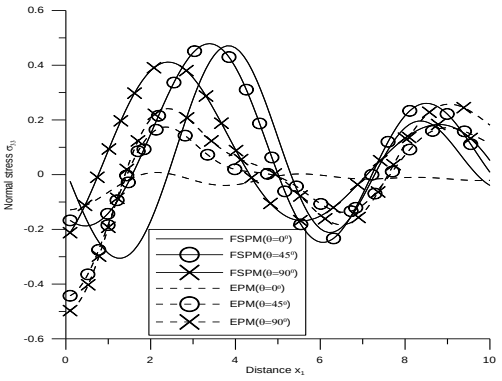

Fig.22
Variation of normal stress σ_{33} w w.r.t distance x_1 due to moving force(frequency domain).

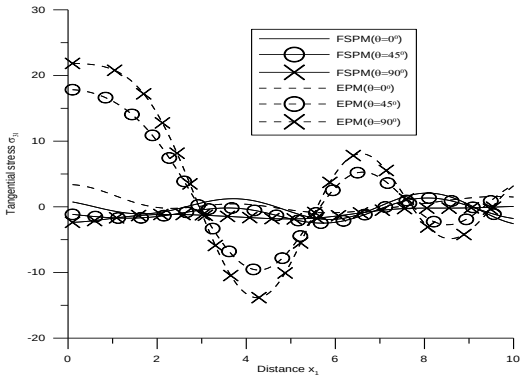

Fig.23
Variation of tangential stress σ_{31} w.r.t distance x_1 due to moving force(frequency domain).

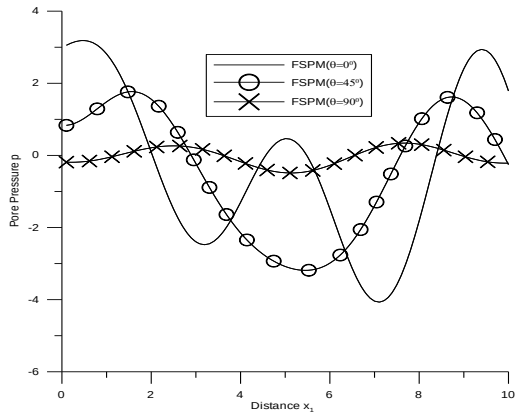

Fig.24
Variation of pore pressure p w.r.t distance x_1 due to moving force (frequency domain).

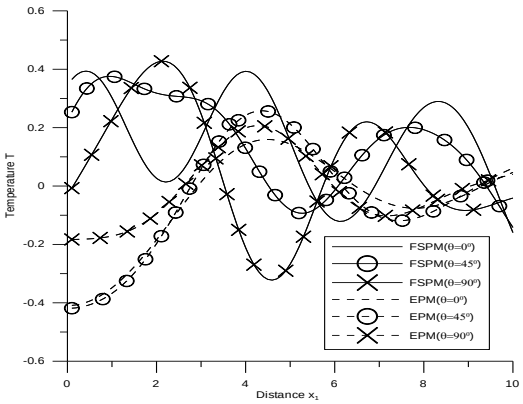

Fig.25
Variation of temperature T w.r.t distance x_1 due to moving force (frequency domain).

7 CONCLUSIONS

Analysis of displacement, stress, pore pressure and temperature change due to concentrated force, uniformly distributed force and a moving force due to inclined load in time and frequency domain is a significant problem of continuum mechanics. Integral transform technique has been used which is applicable to wide range of problems in thermoporoelasticity.

The present investigation is concerned with the deformation of thermoporoelastic half space with incompressible fluid as a result of inclined load of arbitrary orientation. The components of displacement, stress, pore pressure and temperature change are obtained in thermoporoelastic medium due to the various sources by using the Laplace and Fourier transforms. Appreciable porosity effect and effect of change in angle of inclination of inclined load are observed on the components of normal stress, tangential stress, pore pressure and temperature change.

It is observed that for time domain the value of $\sigma_{33}, \sigma_{31}, p, T$ for FSPM oscillates with large magnitude as compared to the values for EPM. Also on the point of application of concentrated force, distributed force and moving force, the porosity effect increases the values of σ_{31} and p while reverse behavior is observed in the values of σ_{33} and T. In frequency domain, it is observed that the trends of variations of stresses, pore pressure and temperature change on the application of concentrated force, distributed force and moving force are similar in nature with significant difference in their magnitude.

All the field quantities are observed to be very sensitive towards the angle of inclination and porosity parameter. Angle of inclination and porosity parameters have oscillatory effects on the numerical value of the physical quantities. The result obtained as a consequence of this research work should be beneficial for researchers working on thermoporoelastic solids. The present study presents a more realistic model for further investigation.

ACKNOWLEDGEMENTS

The authors are thankful to the referee for his valuable comments to improve the manuscript.

REFERENCES

[1] Fillunger P., 1913, Der auftrieb in talsperren, *Osterr Wochenschrift Offentl Baudienst* **19**:532-556.
[2] Terzaghi K.V., 1923, Die berechnug der durchlassigkeitsziffer des tones aus dem verlauf der hydromechanischen spannungserscheinungen, *Sitzungsber Akad Wiss Wien, Math Naturwiss KI , Abt, IIa* **132**:125-138.
[3] Terzaghi K.V., 1925, *Erdbaumechanik auf Bodenphysikalischer Grundlage*, Leipzig-wien, Franz Deuticke.
[4] Terzaghi K.V., 1933, Auftrieb und kapillardruck an betonierten talsperren, *Die Wasserwirtschaft* **26**: 397-399.
[5] Biot M.A., 1941, General theory of three dimensional consolidation, *Journal of Applied Physics* **12**(2): 155-161.
[6] Biot M.A., 1956, Theory of propagation of elastic waves in fluid saturated porous solid I-low frequency range, *Journal of the Acoustical Society of America* **28**:168-178.
[7] Biot M.A., 1956, Theory of propagation of elastic waves in fluid saturated porous solid II-higher frequency range, *Journal of the Acoustical Society of America* **28**:179-191.
[8] Rice J.R. ,Cleary M.P.,1976, Some basic stress diffusion solution for fluid saturated elastic porous media with compressible constituents, *Reviews of Geophysics and Space Physics* **14**:227-241.
[9] Schiffman R. L., 1971, *A Thermoelastic Theory of Consolidation, in Environmental and Geophysical Heat Transfer*, American Society of Mechanical Engineers, New York.
[10] Bowen R. M., 1982, Compressible porous media models by use of the theory of mixtures, *International Journal of Engineering Science* **20**: 697-735.
[11] Noorishad J., Tsang C.F., Witherspoon P. A., 1984, Coupled thermohydraulic-mechanical phenomena in saturated fractured porous rocks: Numerical approach, *Journal of Geophysical Research* **89**:10365-10373.
[12] McTigue D.F., 1986, Thermal response of fluid-saturated porous rock, *Journal of Geophysical Research* **91**(B9): 9533-9542.
[13] Kurashige M., 1989, A thermoelastic theory of fluid-filled porous materials, *International Journal of Solids and Structures* **25**:1039-1052.
[14] Abousleiman Y., Ekbote S., 2005, Solutions for the inclined borehole in a porothermoelastic transversely isotropic medium, *ASME Journal Applied Mechanics* **72**: 102-114.
[15] Bai B., 2006, Fluctuation responses of porous media subjected to cyclic thermal loading, *Computers and geotechnics* **33**:396-403.
[16] Bai B., Li T., 2009, Solution for cylindrical cavity in saturated thermoporoelastic medium, *Acta Mechanica Solida Sinica* **22**(1):85-92.
[17] Jabbari M., Dehbani H., 2010, An exact solution for classic coupled thermoelasticity in axisymmetric cylinder, *Journal of Solid Mechanics* **2**(2):129-143.
[18] Ganbin L., Kanghe X., Rongyue Z., 2010, Thermo-elastodynamic response of a spherical cavity in a saturated poroelastic medium, *Applied Mathematical Modeling* **34**:2213-2222.
[19] Gatmiri B., Maghoul P., Duhamel D.,2010, Two-dimensional transient thermo-hydro-mechanical fundamental solutions of multiphase porous media in frequency and time domains, *International Journal of Solid and Structure* **47**:595-610.
[20] Li X., Chen W., Wang H., 2010, General study state solutions for transversely isotropic thermoporoelastic media in three dimensions and its application, *European Journal of Mechanics - A/Solids* **29**(3): 317-326.
[21] Jabbari M., Dehbani H., 2011, An exact solution for quasi-static poro- thermoelasticity in spherical coordinate, *Iranian Journal of Mechanical Engineering* **12**(1): 86-108.
[22] Liu G., Ding S.,YE R., Liu X., 2011, Relaxation effect of a saturated porous media using the two dimensional generalized thermoelastic theory, *Transport in Porous Media* **86**:283-303.
[23] Belotserkovets b. A., Prevost J. H., 2011, Thermoporoelastic response of fluid-saturated porous sphere: An analytical solution, *International Journal of Engineering Science* **49**(12): 1415-1423.
[24] Bai B., 2013, Thermal response of saturated porous spherical body containing a cavity under several boundary conditions, *Journal of Thermal Stresses* **36**(11): 1217-1232.
[25] Apostolakis G., Dargus G.F., 2013, Mixed variation principal for dynamic response of thermoelastic and poroelastic continua, *International Journal of Solid and Structure* **50**(5): 642-650.
[26] Hou P.F., Zhao M., Jiann-Wen J.U., 2013, The three dimensional green's function for transversely isotropic thermoporoelastic biomaterial, *Journal of Applied Geophysics* **95**: 36-46.
[27] Jabbari M., Hashemitaheri M., Mojahedin A., Eslami M.R., 2014, Thermal buckling analysis of functionally graded thin circular plate made of saturated porous materials, *Journal of Thermal Stresses* **37**:202-220.
[28] Liu M., Chain C., 2015, A micromechanical analysis of the fracture properties of saturated porous media, *International Journal of Solid and Structure* **63**:32-38.

[29] He S.M., Liu W., Wang J., 2015, Dynamic simulation of landslide based on thermoporoelastic approach, *Computers and Geosciences* **75**: 24-32.
[30] Nguyen H.T., Wong H., Fabbri A., Georgin J.F., Prudhomme E., 2015, Analytical study of freezing behaviour of a cavity in thermoporoelastic medium, *Computers and Geotechnics* **67**: 33-45.
[31] Wu D., Yu L., Wang Y., Zhao B., Gao Y., 2015, A refined theory of axisymmetric thermoporoelastic circular cylinder, *European Journal of Mechanics - A/Solids* **53**:187-195.
[32] Kumar R., Ailawalia P., 2005, Moving inclined load at boundary surface, *Applied Mathematics and Mechanics* **26**: 476-485.
[33] Kumar R., Ailawalia P., 2005, Interaction due to inclined load at micropolar elastic half-space with voids, *International Journal of Applied Mechanics and Engineering* **10**:109-122.
[34] Kumar R., Rani L., 2005, Deformation due inclined load in thermoelastic half-space with voids, *Archives of Mechanics* **57**:7-24.
[35] Sharma K., 2011, Analysis of deformation due to inclined load in generalized thermodiffusive elastic medium, *International Journal of Engineering, Science and Technology* **3**(2): 117-129.
[36] Ostsemin A.A., Utkin P.B., 2012, Stress-strain state of a inclined elliptical defect in a plate under biaxial loading, *Journal of Applied Mechanics and Technical Physics* **53**(2): 246-257.
[37] Bogomolov A. N., 2013 , Ushakov A. N., Stress-strain state of an elastic half plane under a system of inclined piecewise-linear loads, *Soil Mechanics and Foundation Engineering* **50**(2): 43-49.
[38] Jabbari M., Dehbani H., 2009, An exact solution for classic coupled thermoporoelasticity in cylindrical coordinate, *Journal of Solid Mechanics* **1**(4): 343-357.
[39] Kumar R., Ailawalia P., 2005, Elastodynamics of inclined loads in micropolar cubic crystal, *Mechanics and Mechanical Engineering* **9**(2): 57-75.